Hydrogen Production from the Steam−Iron Process with Direct Reduction of Iron Oxide by Chemical Looping Combustion of Coal Char

ARTICLE *in* ENERGY & FUELS · JUNE 2008

Impact Factor: 2.79 · DOI: 10.1021/ef800014r

3 AUTHORS, INCLUDING:

Ningsheng Cai
Tsinghua University
136 PUBLICATIONS **1,789** CITATIONS

SEE PROFILE

Hydrogen Production from the Steam−Iron Process with Direct Reduction of Iron Oxide by Chemical Looping Combustion of Coal Char

Jing-biao Yang, Ning-sheng Cai,* and Zhen-shan Li

Key Laboratory of Thermal Science and Power Engineering of Ministry of Education, Department of Thermal Engineering, Tsinghua University, Beijing 100084, China

Received January 7, 2008. Revised Manuscript Received April 19, 2008

Experimental results performed with a fluidized-bed reactor supported the feasibility of the three processes including direct reduction of iron oxide by char, H_2 production by the steam−iron process, and the oxidation of Fe_3O_4 resulting from the steam−iron process to the original Fe_2O_3 by air. Chars resulting from a Chinese lignite loaded with K_2CO_3 were used successfully as a reducing material, leading to the reduction of Fe_2O_3 to FeO and Fe for the steam−iron process, which was confirmed by both the off-gases concentrations and X-ray diffractometer analysis. The reduction of Fe_2O_3 by K-10-char at 1073 K is desirable from the perspective of the carbon conversion rate and high concentration of CO_2. The carbon in char was completely converted to CO_2 when the mass ratio of Fe_2O_3/K-10-char was increased to 10/0.3. The oxidation rate of K-10-char by Fe_2O_3 without a gasifying agent was comparable to the K-10-char steam gasification rate. The fractions of FeO and Fe in the reduced residue were 43 and 57%, respectively, in the case of 3 g of Fe_2O_3 and 0.5 g of K-10-char, which was verified by the total H_2 yield equaling 1000 mL/g K-10-char from the steam−iron process. The time that it took to achieve complete oxidation of Fe_3O_4 to Fe_2O_3 by air with an 8.7% O_2 concentration at 1073 K was about 15 min.

1. Introduction

The current worldwide hydrogen demand is predominantly produced by the steam methane reforming based on natural gas on a large scale.[1,2] However, with increasing prices of oil and natural gas as feedstock, coal and biomass are considered to meet with the growing energy demand.[3,4] Coal gasification combined with a water gas shift (WGS) reaction is considered to be a promising technology for large-scale hydrogen production, but purification of the syngas from CO and CO_2 is needed and will be expensive for the complex process. Therefore, alternative processes for hydrogen production that require none or less purification can be beneficial.

The steam−iron process is one of the oldest methods of producing hydrogen (Figure 1).[3,5] It is a cyclic process for reduction and oxidation of iron oxides, whereby fuel is consumed. For instance, coal is first gasified to syngas, which reacts with iron oxides (hematite Fe_2O_3, magnetite Fe_3O_4, wuestite FeO), resulting into a reduced form of iron oxide (FeO and Fe). Then, the reduced iron oxide reacts with steam to form magnetite and hydrogen. At present, the steam−iron process is not in use for hydrogen production, because other processes are more economically efficient.[1] The level of CO impurity in hydrogen should be 20−50 ppm for the use in fuel cells, such as polymer electrolyte fuel cells (PEFCs);[6] therefore, more attention is paid to the steam−iron process because it can produce hydrogen with high purity.[7–10]

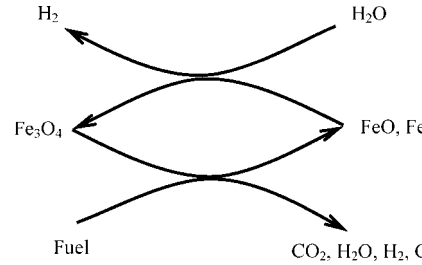

Figure 1. Simplified diagram of the steam−iron process to produce hydrogen.

* To whom correspondence should be addressed. Telephone: 86-10-62789955. Fax: 86-10-62770209. E-mail: cains@tsinghua.edu.cn.

(1) Rostrup-Nielsen, J. R.; Rostrup-Nielsen, T. Large-scale hydrogen production. *CAT THEC* **2002**, *6* (4), 150–159.

(2) Aasberg-Petersen, K.; Bak Hansen, J. H.; Christensen, T. S.; Dybkjaer, I.; Seier Christensen, P.; Stub Nielsen, C.; Winter Madsen, S. E. L.; Rostrup-Nielsen, J. R. Technologies for large-scale gas conversion. *Appl. Catal., A* **2001**, *221* (1−2), 379–387.

(3) Gupta, P.; Velazquez-Vargas, L. G.; Fan, L.-S. Syngs redox (SGR) process to produce hydrogen from coal derived syngas. *Energy Fuels* **2007**, *21* (5), 2900–2908.

(4) Sime, R.; Kuehni, J.; D'Souza, L.; Elizondo, E.; Biollaz, S. The redox process for producing hydrogen from woody biomass. *Int. J. Hydrogen Energy* **2003**, *28* (5), 491–498.

(5) Huebler, J.; Johnson, J. L.; Schora, F. C., Jr.; Tarman, P. B. Production of hydrogen via the steam−iron process. U.S. Patent 3,442,620, 1969.

(6) Hacker, V.; Fankhauser, R.; Faleschini, G.; Fuchs, H.; Friedrich, K.; Muhr, M.; Kordesch, K. Hydrogen production by steam−iron process. *J. Power Sources* **2000**, *86* (1−2), 531–535.

(7) Otsuka, K.; Kaburagi, T.; Yamada, C.; Takenaka, S. Chemical storage of hydrogen by modified iron oxides. *J. Power Sources* **2003**, *122* (2), 111–121.

(8) Otsuka, K.; Yamada, C.; Kaburagi, T.; Takenaka, S. Hydrogen storage and production by redox of iron oxide for polymer electrolyte fuel cell vehicles. *Int. J. Hydrogen Energy* **2003**, *28* (3), 335–342.

(9) Takenaka, S.; Hanaizumi, N.; Son, V. T. D.; Otsuka, K. Production of pure hydrogen from methane mediated by the redox of Ni- and Cr-added iron oxides. *J. Catal.* **2004**, *228* (2), 405–416.

(10) Otsuka, K.; Yamada, C.; Kaburagi, T.; Takenaka, S. Hydrogen storage and production by redox of iron oxide for polymer electrolyte fuel cell vehicles. *Int. J. Hydrogen Energy* **2003**, *28* (3), 335–342.

10.1021/ef800014r CCC: $40.75
Published on Web 06/19/2008

Table 1. Reactions with Thermodynamic Data at 1100 K

number	reactions	$\Delta_f H^0_{(T=1100\ K)}$ (kJ/mol)	$\Delta_f G^0_{(T=1100\ K)}$ (kJ/mol)
1	$C + 3Fe_2O_3 \rightarrow 2Fe_3O_4 + CO$	123.7	−125.8
2	$0.788C + 0.947Fe_3O_4 \rightarrow 3Fe_{0.947}O + 0.788CO$	151.5	−21.7
3	$C + Fe_{0.947}O \rightarrow 0.947Fe + CO$	151.9	−16.1
4	$CO + 3Fe_2O_3 \rightarrow 2Fe_3O_4 + CO_2$	−45.9	−103.6
5	$0.788CO + 0.947Fe_3O_4 \rightarrow 3Fe_{0.947}O + 0.788CO_2$	17.8	−4.2
6	$CO + Fe_{0.947}O \rightarrow 0.947Fe + CO_2$	−17.6	6.1
7	$0.947Fe + H_2O \rightarrow Fe_{0.947}O + H_2$	−16.1	−5.8
8	$3Fe + 4H_2O \rightarrow Fe_3O_4 + 4H_2$	−97.9	−13.7
9	$3Fe_{0.947}O + 0.788H_2O \rightarrow 0.947Fe_3O_4 + 0.788H_2$	−44.4	4.5
10	$4Fe_3O_4 + O_2 \rightarrow 6Fe_2O_3$	−472.6	−166.5

Chemical looping combustion (CLC) with an inherent CO_2 separation advantage is under development.[11–20] In the CLC process, a redox cycle is applied to generate heat by oxidizing a reduced metal or metal oxide (Me_xO_{y-1}) with air to form metal oxide (Me_xO_y) in the air reactor and the metal oxide (Me_xO_y) reacts with the fuel to form CO_2, H_2O, and the reduced metal oxide (Me_xO_{y-1}) in the fuel reactor. Another benefit of CLC is that the energy released in the air reactor can be used as a heat source for an endothermic reaction instead of steam generation.[21–24]

At present, the reduction of metal oxides with coal as fuel is suggested to be conducted by two means. One of them is that coal is first gasified to syngas acting as a reducing fuel,[19,20,25] and another way is that coal gasification and reduction of metal oxide occur in a reactor with gasifying agent.[26,27] In the two means, air separation and steam generation are required, which creates a significant energy penalty, resulting into low efficiency.

If it is assumed that the interaction between solid fuel and oxygen carrier without a gasifying agent can be improved evidently, the system will be much more compact for the metal oxide reduction. Tsuji et al.[28] verified the possibility of the direct reduction of ZnO to Zn by coal without a gasifying agent, and metallic zinc was successfully used to split steam for H_2 production. However, evaporation of ZnO and Zn occurs even under 623 K, leading to trouble for the high conversion of coal under 1173 K.[28] CuO can be reduced to Cu in a direct path by sub-bituminous coal from the experimental results by Cao et al.,[29] but Cu can not realize the function to produce H_2 with steam based on thermodynamics.[3]

There are many metals, such as Ni, Fe, Cu, Co, and Mn, that can be used in CLC.[12–20] However, in the steam−iron process for H_2 production, the metal oxide should have two important characteristics: it should react with fuel to form reduced metal oxide or metallic metal; on the other hand, the reduced form of metal oxide should be regenerable and allow high steam-to-hydrogen conversion.[3] Fe_2O_3 and Fe_3O_4 are the most viable options for use in the steam−iron process. Reduction of iron oxides with hydrocarbons can take place, especially for Fe_2O_3, but is slow for Fe_3O_4 and FeO.[3] Therefore, Fe_2O_3 is especially attractive because it allows complete conversion of syngas as well as high conversion of steam to hydrogen.[3] Further on in this study, Fe_2O_3 was considered. Gupta et al. verified the feasibility of direct reduction of Fe_2O_3 by coal in the thermogravimetric analysis (TGA) experiment under N_2 atmosphere,[30] but it is worthy of further investigation on the direct reduction of Fe_2O_3 by coal in a fluidized bed, which is closer to application.

The main purpose of this study is to reveal the feasibility of the three processes, including Fe_2O_3 reduction by char in a direct path (without a gasifying agent) based on CLC, H_2 production by the steam−iron process, and the oxidation of Fe_3O_4 to the initial Fe_2O_3 by air. Another objective is to obtain some

(11) Ishida, M.; Jin, H.; Okamoto, T. Kinetic behaviour of solid particle in chemical-looping combustion: Suppressing carbon deposition in reduction. *Energy Fuels* **1998**, *12* (2), 223–229.

(12) Jin, H.; Ishida, M. Reactivity study on natural-gas-fueled chemical-looping combustion by a fixed-bed reactor. *Ind. Eng. Chem. Res.* **2002**, *41* (16), 4004–4007.

(13) Lyngfelt, A.; Leckner, B.; Mattisson, T. A fluidized-bed combustion process with inherent CO_2 separation; application of chemical-looping combustion. *Chem. Eng. Sci.* **2001**, *56* (10), 3101–3113.

(14) Mattisson, T.; Lyngfelt, A.; Cho, P. The use of iron oxide as an oxygen carrier in chemical-looping combustion of methane with inherent separation of CO_2. *Fuel* **2001**, *80* (13), 1953–1962.

(15) Abad, A.; Mattisson, T.; Lyngfelt, A.; Johansson, M. The use of iron oxide as oxygen carrier in a chemical-looping reactor. *Fuel* **2007**, *86* (7−8), 1021–1035.

(16) Corbella, B. M.; Palacios, J. M. Titania-supported iron oxide as oxygen carrier for chemical-looping combustion of methane. *Fuel* **2007**, *86* (1−2), 113–122.

(17) Son, S. R.; Kim, S. D. Chemical-looping combustion with NiO and Fe_2O_3 in a thermobalance and circulating fluidized bed reactor with double loops. *Ind. Eng. Chem. Res.* **2006**, *45* (8), 2689–2696.

(18) Readman, J. E.; Olafsen, A.; Smith, J. B.; Blom, R. Chemical looping combustion using $NiO/NiAl_2O_4$: Mechanisms and kinetics of reduction−oxidation (red−ox) reactions from in situ powder X-ray diffraction and thermogravimetry experiments. *Energy Fuels* **2006**, *20* (4), 1382–1387.

(19) Abad, A.; Garcia-Labiano, F.; de Diego, L. F.; Gayan, P.; Adanez, J. Reduction kinetics of Cu-, Ni-, and Fe-based oxygen carriers using syngas ($CO + H_2$) for chemical-looping combustion. *Energy Fuels* **2007**, *21* (4), 1843–1853.

(20) Mattisson, T.; Garcia-Labiano, F.; Kronberger, B.; Lyngfelt, A.; Adanez, J.; Hofbauer, H. Chemical-looping combustion using syngas as fuel. *Int. J. Greenhouse Gas Control* **2007**, *1* (2), 158–169.

(21) Wolf, J.; Yan, J. Parametric study of chemical looping combustion for tri-generation of hydrogen, heat, and electrical power with CO_2 capture. *Int. J. Energy Res.* **2005**, *29* (8), 739–753.

(22) Zafar, Q.; Mattisson, T.; Gevert, B. Integrated hydrogen and power production with CO_2 capture using chemical-looping reforming-redox reactivity of particles of CuO, Mn_2O_3, NiO, and Fe_2O_3 using SiO_2 as a support. *Ind. Eng. Chem. Res.* **2005**, *44* (10), 3485–3496.

(23) Rydén, M.; Lyngfelt, A.; Mattisson, T. Synthesis gas generation by chemical-looping reforming in a continuously operating laboratory reactor. *Fuel* **2006**, *85* (12−13), 1631–1641.

(24) Rydén, M.; Lyngfelt, A. Using steam reforming to produce hydrogen with carbon dioxide capture by chemical-looping combustion. *Int. J. Hydrogen Energy* **2006**, *31* (10), 1271–1283.

(25) Jin, H.; Ishida, M. A new type of coal gas fueled chemical-looping combustion. *Fuel* **2004**, *83* (17−18), 2411–2417.

(26) Dennis, J. S.; Scott, S. A.; Hayhurst, A. N. In situ gasification of coal using steam with chemical looping: A technique for isolating CO_2 from burning a solid fuel. *J. Energy Inst.* **2006**, *79* (3), 187–190.

(27) Leion, H.; Mattisson, T.; Lyngfelt, A. The use of petroleum coke as fuel in chemical-looping combustion. *Fuel* **2007**, *86* (12−13), 1947–1958.

(28) Tsuji, M.; Wads, Y.; Tamaura, Y.; Steinfeld, A.; Kuhn, P.; Palumbo, R. Coal gasification by the coal/CH_4−ZnO−Zn−H_2O solar energy conversion system. *Energy Convers. Manage.* **1996**, *37* (6−8), 1315–1320.

(29) Cao, Y.; Casenas, B.; Pan, W.-P. Investigation of chemical looping combustion by solid fuels. 2. Redox reaction kinetics and product characterization with coal, biomass, and solid waste as solid fuels and CuO as an oxygen carrier. *Energy Fuels* **2006**, *20* (5), 1845–1854.

(30) Gupta, P.; Velazquez-Vargas, L. G.; Li, F.; Fan, L.-S. Chemical looping combustion of coal. In 2005 AIChE Annual Meeting and Fall Showcase, Conference Proceedings, Cincinnati, OH, Oct 30−Nov 4, 2005; pp 7620−7625.

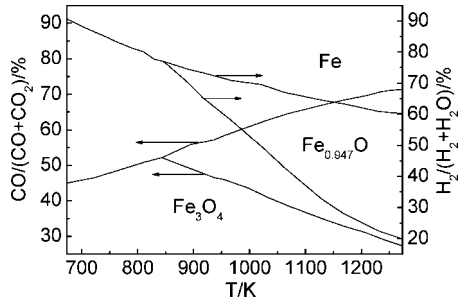

Figure 2. Bauer−Glaessner diagram for the phase change.

preliminary results of the effect of alkali and alkaline earth metal on the gasification of char in the presence of Fe_2O_3 as an oxygen carrier. The potential purity of H_2 and CO_2 from the steam−iron process and CLC using coal as fuel in a direct way is highlighted in this study. In the meantime, the morphology and chemical properties of the iron oxide particles during different processes were characterized using an X-ray diffractometer (XRD) and a scanning electron microscope (SEM) to investigate the chemical properties evolution of iron oxide.

2. Reactions and Thermodynamic Analysis

Wustite is iron-deficient, and the Fe/O ratio in it can range between 0.83 and 0.95.[31] The thermodynamic data used in this study assumes that wustite is present as $Fe_{0.947}O$.[32] Further on in this study, wustite will be denoted as $Fe_{0.947}O$ when used in thermodynamic calculations and as FeO in all other situations. Only carbon is considered as the main constituent in the char, and the relevant reactions involved in the three processes are listed in Table 1; therefore, reactions 1−6 occur in the Fe_2O_3 reduction process. Reactions 7−9 occur in the steam−iron process, and reaction 10 occurs in the oxidation of Fe_3O_4 by air. Thermodynamic data were taken from thermochemical data of pure substances.[32] The reduction reactions of hematite, magnetite, and wustite by carbon are endothermic. The reduction of magnetite with CO to wustite is also endothermic, except for the reduction of hematite to magnetite and wustite to metal iron with CO. According to thermodynamics carbon reduces Fe_2O_3 into Fe_3O_4 at temperatures > 600 K, reduces Fe_3O_4 into FeO, and reduces FeO into Fe at temperatures > 1000 K for $\Delta_f G^0 < 0$. The formed CO in reactions 1−3 in Table 1 can react further and contribute to the reduction via reactions 4−6.

The equilibrium constants for the reactions between the iron oxides and H_2−H_2O or CO−CO_2 determine the ratio between H_2/H_2O and CO/CO_2 at equilibrium and, thus, the maximum CO conversion in the reduction of Fe_2O_3 and the maximum H_2O conversion in the steam−iron process. From the Bauer−Glaessner diagram as shown in Figure 2, it can be seen that $Fe_{0.947}O$ is stable above temperatures of 843 K, but at lower temperatures, it is thermodynamically favored to convert Fe_3O_4 directly into Fe.[33,34] The conversion of Fe_3O_4 takes place until the gas phase reaches 40 vol % CO when the temperature is higher than 673 K. For example, a CO/CO_2 gas mixture with 50 vol % CO at 1073 K has a reducing capacity to convert magnetite into wustite but cannot reduce wustite to metal iron. The reducing capacity to convert wustite to metal iron requires a CO/CO_2 gas mixture with 65 vol % CO at 1073 K. The Bauer−Glaessner diagram clearly shows that the total hydrogen production in the steam−iron process is limited by the ratio of H_2O to H_2. Furthermore, the Bauer−Glaessner diagram shows that a higher equilibrium conversion of steam to hydrogen is expected when metal iron is formed during reduction, and the conversion of steam with Fe and $Fe_{0.947}O$ to H_2 is higher with lower temperatures, which is beneficial for the efficiency of the process. The reaction rate, however, will be slower at lower temperatures.

3. Experimental Section

3.1. Preparation of Test Samples. Details of the preparation of Fe_2O_3 particles used have been given previously;[35] these are summarized here in brief. The oxygen carrier was prepared from Fe_2O_3 powder from the manufacturer Shantou Xilong Chemical Factory, China, with a purity of 99.9%. The received Fe_2O_3 powder was sieved to a size range of 200−450 μm. The particles of Fe_2O_3 were then heated to 1173 K and maintained at this temperature for 5 h. The calcinated particles were then sieved to 200−450 μm. The BET area of the calcinated Fe_2O_3 particles is 1.35 m^2/g determined by a Micromeritics micropore analyzer, ASAP2010. The calcinated Fe_2O_3 was used as the fresh oxygen carrier in this study.

The chars produced from the Baorixile lignite (BL), which was a Chinese low-rank coal from opencast mine, were used for the main purpose of this study to investigate the reduction of Fe_2O_3 by char in a direct path (without a gasifying agent). The proximate and ultimate analyses of the parent coal are listed in Table 2. Coal samples were sieved to a size range of 200−450 μm. The removal of mineral matter from coal by acid treatment (demineralization) is accompanied by structural changes, which alters the nature and, thus, the behavior during gasification.[36,37] Therefore, in this study, the catalyst was added to the raw coal directly (without destructive pretreatment) by impregnation with the following procedure: analytical-grade anhydrous K_2CO_3 (from Beijing Chemical Factory, China) and $Ca(NO_3)_2 \cdot 4H_2O$ (from Shantou Xilong Chemical Factory, China) were employed as the precursors for catalyst; then coal (10 g) was added to 30 mL aqueous solutions of the above salts; and at last, the slurry was stirred for 3 h at ambient temperature and dried in air overnight at 378 K. The catalyst loading was 0−10% in terms of the mass ratio of metal/coal.

The chars were prepared as follows: all samples were devolatilized in a fluidized-bed reactor shown in Figure 3 under a flow rate of 300 mL/min Ar with a purity of 99.995% at a heating rate of 30 K/min from room temperature to a final temperature of 1173 K, and the soaking time was 30 min. The chars recovered were then sieved to the size range of 200−450 μm for use in this study. The reactivity of a char is known to be influenced by its heating treatment history,[26] but the reactivity of a char hardly changes under such a temperature of 1173 K from published results[38,39] and preliminary results obtained in the previous study.[35] Hence, this method of preparing the chars is sufficient for the measurements of the reactivity of the chars.[26] The chars produced from the parent coal and coal loaded with K and Ca are denoted as raw-char, K-2-char, K-5-char, K-10-char, and Ca-10-char, respectively, whereby the number following the metal is the percentage of catalyst loading, and their ultimate analysis are given in Table 3.

3.2. Experimental Setup. The three processes, including the Fe_2O_3 reduction by char in a direct path, H_2 production by the steam−iron process, and the oxidation of Fe_3O_4 to Fe_2O_3 by air, were carried out under atmospheric pressure using a fluidized-bed apparatus as shown in Figure 3. The fluidized-bed reactor was made of quartz, which had a total length of 850 mm. Samples were placed on a porous plate located at 390 mm from the bottom of the reactor.

Table 2. Proximate and Ultimate Analyses of the Coal Sample

	proximate analysis (wt %, ad basis)				ultimate analysis (wt %, ad basis)				
sample	inherent moisture (M)	ash (A)	volatile matter (VM)	fixed carbon (FC)	C	H	N	S	O (diff)
BL	3.89	10.89	37.31	47.91	63.09	4.17	0.96	0.33	31.45

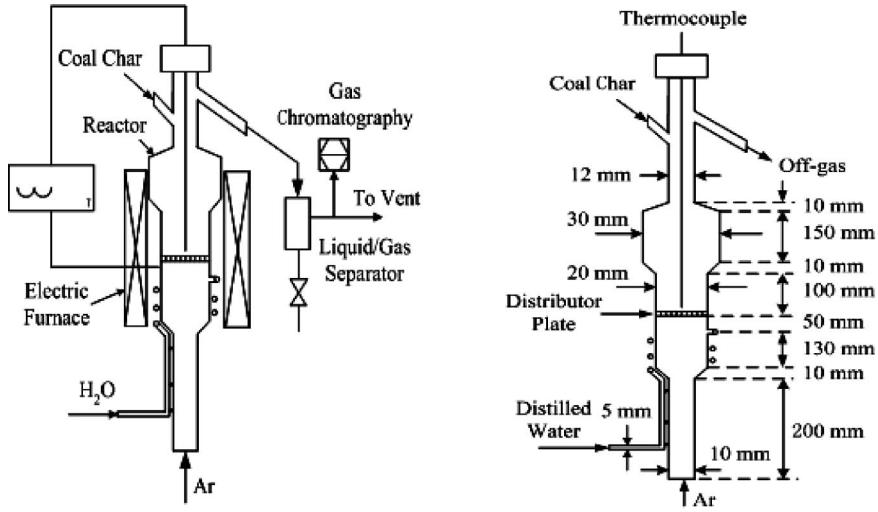

Figure 3. (a) Schematic diagram of the reaction system and (b) details of the fluidized-bed reactor.

Table 3. Ultimate Analysis of Char Samples (wt %, ad basis)

samples	C	H	N	O and S (by diff)
raw-char	74.87	0.42	0.65	24.06
K-2-char	77.54	0	0.84	21.62
K-5-char	68.19	0.19	0.52	31.10
K-10-char	62.57	0	1.07	36.36
Ca-10-char	60.62	0	1.19	38.19

The diameter of the main reaction range is constant for 20 mm, after which a disengaging section of 30 mm in diameter is placed. This disengaging section was designed to avoid smaller particles from leaving the reactor. The temperature was measured 5 mm above and 5 mm under the distributor plate by using a K-type thermocouple enclosed in a stainless-steel pipe with a diameter of 3 mm. The temperature under the plate was used to control the reactor temperature. All reactor temperatures in this study referred to the temperature measured above the plate, and the thermocouple above the plate was immersed in the bed materials. Ar was used as fluidizing gas because Ar was required as the carrier gas for gas chromatography (GC). The flow rate of carrier argon was controlled by a mass flowmeter. The purity of Ar in this study was always 99.995%. The reactor was heated by an electric furnace. In the steam−iron process, distilled water was introduced from the bottom of the reactor by a pump (2PB10C, China Spacesat Co., Ltd.). The high-temperature steam was generated by forcing water through an evaporator section containing quartz coil twisted around the quartz tube under the plate as shown in Figure 3b. The water was guarantied to evaporate completely. On the other hand, the pressure measured by a pressure gauge linking to the reactor was stable, indicating that the steam was stable in the reactor.[35] Therefore, a continuous flow of steam was guarantied in this study. The high-temperature steam passed through the plate, and was then allowed to flow out the reactor to a cooling section, which was made of a stainless-tube coil; at last, steam was condensed back to water and separated from product gases by a liquid/gas separator.

During direct reduction of Fe_2O_3 by char and the steam−iron process, the gases after the liquid/gas separator were led to a gas analyzer TCD−GC (Perkin-Elmer, Auto System XL) where the actual concentrations of H_2, CO, CH_4, and CO_2 were measured. The actual gas concentrations analyzed in this study have excluded the steam. The off gases of H_2, CO, CO_2, and CH_4 were sampled every 3.5 min by GC. During oxidation of Fe_3O_4 to Fe_2O_3 by the air, the off gases were analyzed by an oxygen analyzer (Photon, MADUR) and the O_2 concentrations were recorded every 12 s.

The experimental conditions for the three processes and steam/CO_2 gasification of char are summarized in Table 4. The reduction of Fe_2O_3 by char was carried out by five test series. For series I−IV, samples of chars and Fe_2O_3 particles were thoroughly mixed and placed on the porous plate and then heated in an inert atmosphere of fluidizing Ar from room temperature to 1173 K. Series I: Fe_2O_3 was reduced by raw-char, Ca-char, and K-char. In this series, the mass of Fe_2O_3 and chars were maintained at 3 and 0.5 g, respectively, and the flow rate of Ar was maintained at 426 mL/min. Series II: Fe_2O_3 was reduced by K-10-char directly. In this series, the mass of Fe_2O_3 and chars were maintained at 3 and 0.5 g, respectively, and the flow rate of Ar was changed with three different values (142, 284, and 426 mL/min). Series III: Fe_2O_3 was reduced by K-10-char with a different mass ratio of Fe_2O_3 to K-10-char. In this series, the flow rate of Ar was 142 mL/min. Series IV: Fe_2O_3 was reduced by K-char with different K loadings. In series IV, the mass of Fe_2O_3 and chars were maintained at 5 and 0.3 g, respectively, and the flow rate of Ar was 142 mL/min. Series V: Fe_2O_3 was reduced by K-10-char with different final temperatures. In this series, the mass of Fe_2O_3 and chars were maintained at 5 and 0.3 g, respectively, the sample was heated under 142 mL/min Ar to a set temperature, and the temperature was stabilized until the complete conversion of char by iron oxide. The bed height of 3 g of Fe_2O_3 and 0.5 g of K-10-char was approximately 15 mm when the bed was not fluidized. When the bed is fluidized by 300 mL/min (normalized to 0.1 MPa and 273.15 K) of Ar, this

Table 4. Experimental Conditions for Different Processes

process	series	temperature range (K)	ratio of Fe_2O_3/char	flow rate of Ar or reacting agent (mL/min)
	I	298−1173	3/0.5 (different chars)	426 Ar
	II	298−1173	3/0.5 (K-10-char)	142/284/426 Ar
Fe_2O_3 reduction by char	III	298−1173	3/0.5, 5/0.3, 10/0.3 (K-10-char)	142 Ar
	IV	298−1173	5/0.3 (chars with different K loading)	142 Ar
	V	298−1023/1073/1173	5/0.3 (K-10-char)	142 Ar
steam char gasification		1073	0.3 g of K-10-char	142 (Ar)/162 (steam)
char−CO_2 gasification		1073	0.3 g of K-10-char	142 (Ar)/162 (CO_2)
Fe_2O_3 reduction by char with CO_2		298−1173	3/0.5 (K-10-char)	284 (Ar)/20 (CO_2)
steam−iron process		1073	3/0.5 and 3/0.28	142 or 284 (steam)
Fe_3O_4 oxidation by air		1073	3/0.5	142 (Ar)/100 (air)

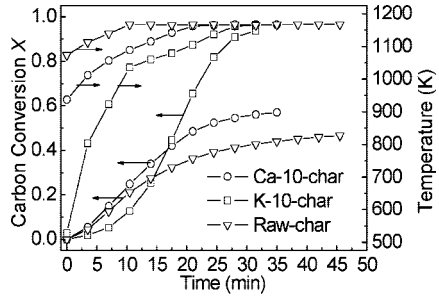

Figure 4. Carbon conversion of chars in the Fe_2O_3 reduction process.

corresponds to a velocity ratio, u/u_{mf}, of 13 and 18 for the Fe_2O_3 particles and char, respectively, where u and u_{mf} are the gas velocity and the minimum fluidization velocity, respectively.

In the steam−iron process, when the Fe_2O_3 reduction process completed, the fluidizing Ar was tuned to 284 or 142 mL/min and the reactor temperature was lowered. Once the temperature was stabilized at 1073 K, 0.13 g/min of water was introduced from the bottom of the reactor as illustrated in Figure 3.

In the oxidation of Fe_3O_4 to Fe_2O_3 by air, when the steam−iron reaction completed, the water feed was stopped, the fluidizing Ar was maintained at 142 mL/min, and the reactor temperature was stabilized at 1073 K. Once the reactor was purged clean by Ar, a gas mixture with 8.7 vol % O_2 resulting from 142 mL/min of Ar, and 100 mL/min of air with 99.995% purity was introduced to avoid an excessive temperature increase.

3.3. Data Evaluation. The actual concentrations of H_2, CO, CO_2, and CH_4 in the outlet gases are measured by GC, and the actual concentration of Ar in the outlet gas can be calculated. The Ar flow (known by a mass flowmeter) is divided by the concentration of Ar to obtain the total flow of the off gases. The total flow of the off gases is multiplied by the concentrations of H_2, CO, CO_2, and CH_4 to obtain the flow of H_2, CO, CO_2, and CH_4. Then, the masses of CO, CO_2, and CH_4 converted up until the time t are calculated by integration using the Simpson method, and the total amount of carbon in the outlet gases can be obtained. At last, the total mass of carbon in the outlet gases is divided by the total amount of carbon in the original char to obtain the carbon conversion X as follows:[27,39]

$$X = \frac{m_{CO} + m_{CO_2} + m_{CH_4}}{m_{total}} \quad (1)$$

where m_{total} is the total amount of carbon in the original char, m_{CO}, m_{CO_2}, and m_{CH_4} are the mass of carbon in the products CO, CO_2, and CH_4 converted up until the time t, and t is the time elapsed since the start of the reduction period.

3.4. XRD and SEM Analysis. An X-ray diffractometer (Bruker D8 Advance) using Cu Kα radiation (40 kV and 40 mA) was used to analyze the samples of iron oxide and char. The samples were scanned in a step-scan mode, with a step size of 0.02° over the angular 2θ range of 10−80°.

The morphological features of iron oxide samples after different reactions were characterized by a scanning electron microscope (SEM, KYKY-2800). The electron beam energy was 20 kV. In most cases, magnifications at 3000× were selected to be analyzed.

4. Results and Discussion

4.1. Direct Reduction of Fe_2O_3 by Char. Figure 4 shows the carbon conversion of different chars in the Fe_2O_3 reduction in series I. The mass of Fe_2O_3 and char was fixed at 3 and 0.5 g, respectively. At 30 min, the K-10-char reaches 92% conversion and the conversions of Ca-10-char and raw-char are 52 and 40%, respectively. It is evident that K-10-char can be completely oxidized by Fe_2O_3. The temperature profiles in Figure 4 show that the beginning reduction temperatures of K-10-char, Ca-10-char, and raw-char with Fe_2O_3 are about 773, 950, and 1073 K, respectively. The reactivity of K-10-char was high; therefore, the following experiments focused on the Fe_2O_3 reduction by K-char.

The gases distribution for the case that Fe_2O_3 was reduced by K-10-char with different flow rates of Ar is shown in Figure 5a. Experiments of series II were designed to change the residence time of CO, but the results indicate that the flow rate of Ar does not change the trend that the CO concentration becomes higher than that of CO_2 once the temperature exceeds 1073 K as shown in Figure 5a. The carbon conversions of K-10-char are the same irrespective of the flow rate of Ar based on the results in Figure 5b. To obtain high-purity CO_2, CO resulting from the reaction between char and Fe_2O_3 is needed to be subsequently oxidized by iron oxide. When the temperature is lower than 1050 K, the gas product is mainly of CO_2 because the generation rate of CO is lower than the oxidation rate of CO by iron oxide.[35] When the temperature is increased, the rate of CO production is accelerated significantly and the fresh iron oxide is depleted, resulting into the escape of CO from the bed materials related to the gas−solid mixing in the fluidized bed. Another reason for the high CO_2 concentration at the start of the reduction is probably caused by the fact that fresh Fe_2O_3 is reacting with the char. When fresh Fe_2O_3 is reduced to Fe_3O_4, the conversion of char to CO_2 will become more difficult, resulting into the increase of the formation rate of CO. It can be explained that the reduction of Fe_2O_3 by char in a direct path includes the reaction process of carbon with iron oxide to produce CO and the reduction process of iron oxide by CO to produce CO_2.

As shown in Figure 2, the CO/CO_2 gas mixture with 50 vol % CO at 1073 K has a reducing capacity to convert magnetite into wustite but cannot reduce wustite to metal iron. A reducing capacity to convert wustite to metal iron requires a CO/CO_2 gas mixture with 65 vol % CO at 1073 K. From the results in Figure 5a, under kinetic control conditions, the fraction of CO is 56.7 vol % at 1073 K; therefore, the CO/CO_2 gas mixture has a reducing capacity to convert magnetite into wustite. When the temperature is higher than 1073 K, the fraction of CO is larger than 67 vol % as shown in Figure 5a; therefore, it has a reducing capacity to convert wustite to metal iron because the CO/CO_2 gas mixture with 68.2 vol % CO at 1173 K has a capacity to convert wustite to metal iron.

(31) Hacker, V.; Faleschini, G.; Fuchs, H.; Fankhauser, R.; Simader, G.; Ghaemi, M.; Spreitz, B.; Friedrich, K. Usage of biomass gas for fuel cells by the SIR process. *J. Power Sources* **1998**, *71* (1−2), 226–230.

(32) Barin, I. *Thermochemical Data of Pure Substances*, 3rd ed.; Cheng, N. L., Niu, S. T., Xu, G. Y., et al., Eds.; Science Press: Beijing, China, 2003.

(33) Oeters, F. Iron. *Ullmann's Encyclopedia of Industrial Chemistry*, 7th ed.; John Wiley and Sons: New York, 2006.

(34) Bleeker, M. F.; Kersten, S. R. A.; Veringa, H. J. Pure hydrogen from pyrolysis oil using the steam−iron process. *Catal. Today* **2007**, *127* (1−4), 278–290.

(35) Yang, J.-B.; Cai, N.-S.; Li, Z.-S. Reduction of iron oxide as an oxygen carrier by coal pyrolysis and steam char gasification intermediate products. *Energy Fuels* **2007**, *21* (6), 3360–3368.

(36) Onal, Y.; Ceylan, K. Effects of treatments on the mineral matter and acidic functional group contents of turkish lignites. *Fuel* **1995**, *74* (7), 972–977.

(37) Lemaignen, L.; Zhuo, Y.; Reed, G. P.; Dugwell, D. R.; Kandiyoti, R. Factors governing reactivity in low temperature coal gasification. Part II. An attempt to correlate conversions with inorganic and mineral constituents. *Fuel* **2002**, *81* (3), 315–326.

(38) Sharma, A.; Kadooka, H.; Kyotani, T.; Tomita, A. Effect of microstructural changes on gasification reactivity of coal chars during low temperature gasification. *Energy Fuels* **2002**, *16* (1), 54–61.

(39) Sekine, Y.; Ishikawa, K.; Kikuchi, E.; Matsukata, M.; Akimoto, A. Reactivity and structural change of coal char during steam gasification. *Fuel* **2006**, *85* (2), 122–126.

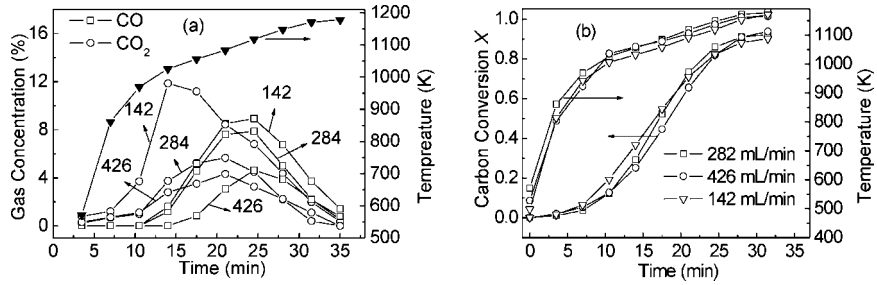

Figure 5. Gases concentration and carbon conversion of K-10-char with different flow rates of Ar.

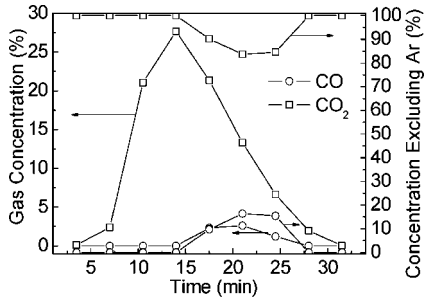

Figure 6. Gas concentration resulting from 5 g of Fe_2O_3 and 0.3 g of K-10-char.

Another method to extend the residence time of gas products in the fluidized bed is to increase the mass ratio of Fe_2O_3/char, and series III were designed to demonstrate this purpose. Figure 6 gives the gases distribution with time resulting from 5 g of Fe_2O_3 and 0.3 g of K-10-char, and the temperature profile is identical to that in Figure 5. Figure 6 shows that the CO_2 concentration is higher than that of CO during the whole process and the CO_2 concentration excluding Ar is almost larger than 90%. When the mass ratio of Fe_2O_3/K-10-char is increased to 10/0.3, the carbon in char is completely converted to CO_2 and the CO_2 purity is nearly 100% during the whole process. Therefore, increasing the mass ratio of Fe_2O_3 to char is a better way to control the CO/CO_2 ratio. This is also strengthened by the conclusion draw by Gupta et al. that the addition of excess iron oxide would maximize the conversion of CO.[3]

The Fe_2O_3 conversion α is defined as follows by neglecting oxygen from char based on the fact that complete reduction of Fe_2O_3 is achieved when all Fe_2O_3 is converted to Fe:

$$\alpha = \frac{(16/28)m_{CO} + (32/44)m_{CO_2}}{(48/160)m_{Fe_2O_3}} \times 100\% \qquad (2)$$

where m_{CO} and m_{CO_2} and are the mass of CO and CO_2 converted up until the time t and $m_{Fe_2O_3}$ is the mass of Fe_2O_3 at the beginning.

For the case of 3 g of Fe_2O_3 and 0.5 g of K-10-char, the conversion of Fe_2O_3 is 70.2% based on the results in Figure 5 using the conversion α defined above. For the case of 5 g of Fe_2O_3/0.3 g of K-10-char and 10 g of Fe_2O_3/0.3 g of K-10-char, the conversions of Fe_2O_3 are 32.4 and 16.1%, respectively. The conversions of Fe_2O_3 to Fe_3O_4 and to FeO are 11.1 and 33.3%, respectively; therefore, in the case of 10 g of Fe_2O_3 and 0.3 g of K-10-char, Fe_3O_4/FeO may be formed in the reduction process. It means that low conversion of Fe_2O_3 is favorable for a high concentration of CO_2.

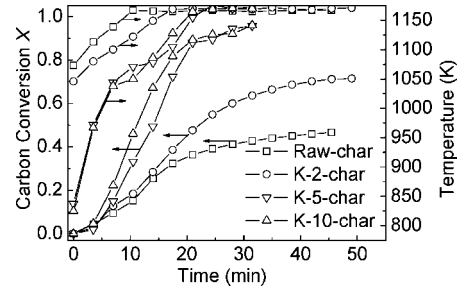

Figure 7. Carbon conversion of chars with different K loadings.

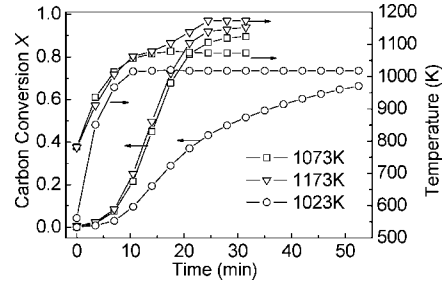

Figure 8. Carbon conversion of K-10-char at different final temperatures.

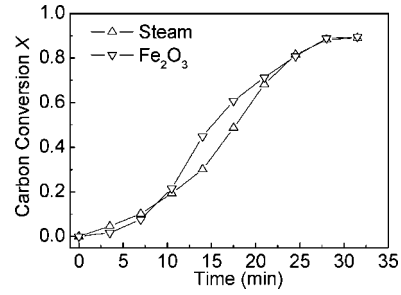

Figure 9. Carbon conversion of K-10-char oxidized by steam and Fe_2O_3, respectively.

The results from series I to III indicated that K-10-char can be completely converted to CO_2 and CO by Fe_2O_3 in a direct way. However, from the perspective of economics, it is necessary to investigate the K loading effect on the conversion of char. This is the main purpose of experiments in series IV. Carbon conversions of K-chars with different loadings and temperature profiles are shown in Figure 7. At a given reaction time, the conversion increases with K loading, but there is no considerable difference between K-5-char and K-10-char in carbon conversion, indicating that a loading between 5 and 10% can be chosen for the complete conversion of K-char by Fe_2O_3.

Table 5. XRD Spectral Data of Fe Species from the XRD Library

species	Fe_2O_3			Fe_3O_4				FeO		Fe	
2θ (deg)	33.4	35.8	54.5	30.1	35.5	57.0	62.6	36.1	41.9	60.7	44.7	65.0
relative intensity (%)	100	72	40	29	100	24	34	67	100	46	100	20

The delicate effect of K_2CO_3 on the Fe_2O_3 reduction by K-char may be related to the low melting point of K_2CO_3 being 1164 K.[40] It was well-known that potassium compounds tend to be mobile and redistribute themselves during char gasification, maintaining catalytic activity throughout the whole gasification process.[41]

On the basis of the results from series I to IV, 80% of carbon in K-10-char was converted to gas until 1073 K; in the meantime, the CO concentration is significantly lower than that of CO_2 when the temperature is lower than 1073 K. Another advantage of the reduction of Fe_2O_3 by K-char under the temperature below 1173 K is that the melting of K_2CO_3 in K-char is avoided, which is favorable for the smooth operation of iron oxide particles in a moving bed or a bubbling fluidized bed.

Figure 8 shows the carbon conversion of K-10-char at different final temperatures performed in series V. The carbon conversion curves are almost identical before 1073 K, but the difference between 1073 and 1173 K is only about 5%. Therefore, reduction of Fe_2O_3 by K-10-char at 1073 K is desirable from the perspective of the carbon conversion rate and high concentration of CO_2. However, the carbon conversion for the case with a final temperature of 1023 K is only 60% after 50 min, suggesting that the interaction between Fe_2O_3 and K-10-char is week because K_2CO_3 in K-10-char does not become softening sufficiently. Another reason for the low carbon conversion of K-10-char at a low temperature with 1023 K may be caused by the slower reaction rate of K-10-char with Fe_3O_4 to FeO/Fe.

An additional set of experiments as shown in Table 4 was conducted to investigate the difference between the K-10-char steam gasification and Fe_2O_3 reduction by K-10-char. In the case of Fe_2O_3 reduction by K-10-char, the conditions are just as that in series V, and the final temperature is 1073 K. In the case of steam gasification of K-10-char, 0.3 g of K-10-char without Fe_2O_3 was heated to 1073 K under 142 mL/min of Ar. When the temperature was stabilized at 1073 K, 0.13 g/min of water was introduced from the bottom of the reactor. The carbon conversion of K-10-char during steam gasification is almost identical to that of K-10-char oxidized by Fe_2O_3 as shown in Figure 9, indicating that the oxidation rate of K-10-char by Fe_2O_3 without a gasifying agent is at least equivalent to or higher than the K-10-char steam gasification rate for Fe_2O_3 reduction by K-10-char in a temperature ramp to 1073 K. Furthermore, the experimental results also indicated the carbon conversion of K-10-char with CO_2 as a gasifying agent in a given time was always lower than that of steam gasification when the partial pressure of the gasifying agent and temperature were identical as shown in Table 4, which agreed with the well-known fact that steam reacts faster with char than CO_2.[42]

The 2θ angles and relative intensity of Fe_2O_3, Fe_3O_4, FeO, and Fe from the XRD library are listed in Table 5 to distinguish different Fe species in the iron oxide sample. Figure 10 shows the XRD spectra of fresh Fe_2O_3 particles, where the discrete vertical lines are the standard spectra of Fe_2O_3 from the XRD library. The XRD spectra of the Fe_2O_3 residue after reduction

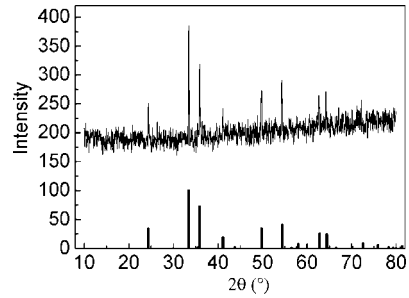

Figure 10. XRD spectra of the fresh Fe_2O_3 sample.

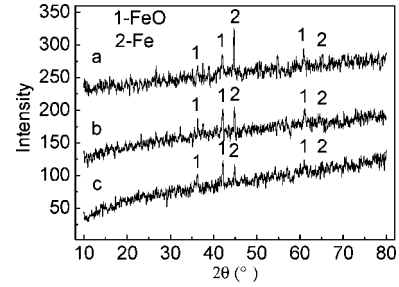

Figure 11. XRD spectra of the Fe_2O_3 residue after reduction by chars: (a) 3 g of Fe_2O_3 reduced by 0.5 g of K-10-char, (b) 3 g of Fe_2O_3 reduced by 0.5 g of Ca-10-char, and (c) 3 g of Fe_2O_3 reduced by 0.5 g of raw-char.

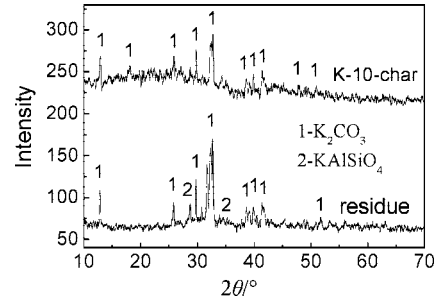

Figure 12. XRD spectra of K-10-char and the residue of K-10-char after Fe_2O_3 reduction.

by raw-char, Ca-10-char, and K-10-char are shown in Figure 11, where there are peaks corresponding to 36.1°, 41.9°, and 60.7° in 2θ belonging to FeO and peaks at 44.7° and 65° belonging to Fe. There are no Fe_2O_3 and Fe_3O_4 species in Figure 11, indicating that Fe_2O_3 was reduced to FeO and Fe by chars. Furthermore, it provides promising prospect to produce H_2 through the steam−iron process based on reactions 7−9 as shown in Table 1. If it is assumed that Fe_2O_3 is reduced to Fe and FeO as follows:

$$2C + Fe_2O_3 \rightarrow 2Fe + CO + CO_2 \quad (3)$$

$$C + 3Fe_2O_3 \rightarrow 6FeO + CO + CO_2 \quad (4)$$

the stoichiometry mass ratio of K-10-char/Fe_2O_3 for eqs 3 and 4 is 0.72/3 and 0.36/3, respectively; therefore, it is expected that Fe_2O_3 can be reduced to FeO and Fe in the case of 0.5 g of K-10-char and 3 g of Fe_2O_3.

The amounts of Na_2O and K_2O in the ash of parent coal are 0.86 and 0.38%, respectively. Therefore, K transformation is the focus because the K loading is 10% in terms of the mass ratio of K/coal in the case of K-10-char. The XRD spectra of K-10-char and the residue of K-10-char after Fe_2O_3 reduction in the case of 0.5 g of K-10-char and 3 g of Fe_2O_3 are shown in Figure 12. Peaks for carbon were not observed, and peaks were almost attributed to K_2CO_3 for K-10-char. It was suggested that the surface of K-10-char was covered with dense K_2CO_3

(40) McKee, D. W.; Spiro, C. L.; Kosky, P. G.; Lamby, E. J. Eutectic salt catalysts for graphite and coal char gasification. *Fuel* **1985**, *64* (6), 805–809.

(41) Godavarty, A.; Agarwal, A. Distribution and catalytic activity of eutectic salts in steam gasification of coal. *Energy Fuels* **1999**, *14* (3), 558–565.

(42) van Heek, K. H.; Mühlen, H. J. *Chemical Kinetics of Carbon and Char Gasification, Fundamental Issues in Control of Carbon Gasification Reactivity*; Lahaye, J., Ehrburger, P., Eds.; Kluwer Academic Publishers: Dordrecht, The Netherlands, 1991; pp 1−34.

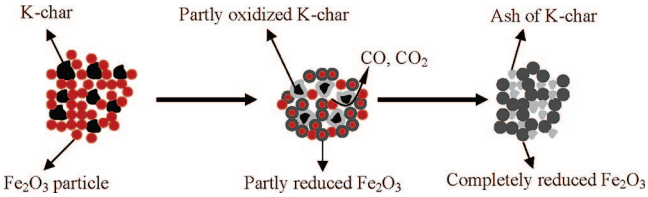

Figure 13. Evolution of Fe_2O_3 reduction by K-char.

dispersing uniformly on it; therefore, peaks corresponding to carbon could not be detected by XRD. Water-insoluble compound $KAlSiO_4$ was found for the residue of K-10-char, and no peaks corresponding to Fe species were observed.

It is suggested that the reduction of Fe_2O_3 by K-char with suitable loading is in accordance with the following evolution as shown in Figure 13. The K-char becomes softened when the temperature increases, and then the Fe_2O_3 particles surrounding the K-chars adhere to the K-char, resulting into the formation of CO, which is then oxidized by the iron oxide to form CO_2. The contact efficiency between char and Fe_2O_3 particles is accelerated with the mobile effect of potassium compounds. Ash of K-char may stick on the iron oxide surface, but no compositions of the ash were detected from the XRD spectra of residue of Fe_2O_3 after reduction as shown in Figure 11.

K_2CO_3 and $Ca(OH)_2$ are regarded as preferable catalysts because of their high activity and fair abundance for availability.[43–45] In 1970s, the Exxon catalytic coal gasification process using K_2CO_3 as a catalyst was developed. However, the process has not yet achieved commercial operation in part because of a fatal demerit of the process, which is the additional cost of the catalyst.[44,46] Furthermore, K_2CO_3 interacts with mineral matter in coal, resulting in water-insoluble compound $KAlSiO_4$ as shown in Figure 12, which makes recycled use of the catalyst and disposal of the ash difficult.[47,48] K_2CO_3 could be saved by pretreatment of the coal with $Ca(OH)_2$, which reacts with mineral matter preferentially to form gehlenite.[47] In recent years, more and more attention has been focused on the catalytic activity of black liquid for its high alkaline composition.[49] Experimental results indicated that black liquid has a high activity for steam gasification of coal.[50] With a cheap catalyst source, black liquid, and operation experience in the Exxon catalytic coal gasification process, an economic operation for catalytic gasification is expectable.

In the experiments from series I to V, Fe_2O_3 was reduced directly by chars under an inert atmosphere. From the thermodynamic consideration, high-purity CO_2 can be obtained with

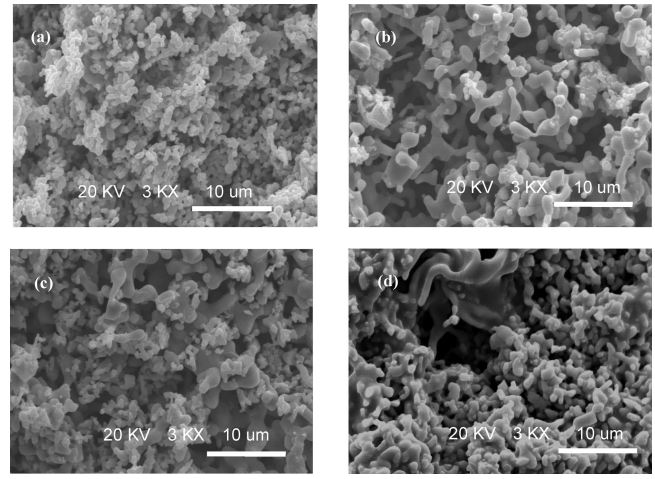

Figure 14. SEM images of Fe_2O_3 under different treatment: (a) fresh Fe_2O_3 particle after preparation, (b) reduction residue of 3 g of Fe_2O_3 by 0.5 g of K-10-char at the final temperature of 1173 K, (c) reduction residue of 3 g of Fe_2O_3 by 0.5 g of raw-char at the final temperature of 1173 K, and (d) reduction residue of 3 g of Fe_2O_3 by 0.5 g of K-10-char at the final temperature of 1023 K.

reduction of Fe_2O_3 to Fe_3O_4. The reduction of Fe_3O_4 to FeO and Fe can be realized by controlling the ratio of CO/CO_2 based on the Bauer−Glaessner diagram in Figure 2, but pure CO_2 cannot be obtained when Fe_3O_4 is further reduced with the carbon. An additional set of experiments as shown in Table 4 was conducted to investigate the effect of CO_2 as a fluidizing agent. A mixture of 284 mL/min Ar and 20 mL/min CO_2 was introduced with other conditions identical to series II. It was found that Fe_2O_3 was reduced to FeO, but the fraction of CO was about 0.6, indicating that a considerable amount of CO cannot be oxidized to CO_2, which leads to another troublesome area. This can be resolved by countercurrent operation in a moving bed, as stated by Gupta et al. that the addition of excess iron oxide would maximize the conversion of CO.[3] However, an increase in the ratio of iron oxide/fuel will leads to a low conversion of iron oxide particles.

SEM images of Fe_2O_3 under different treatments with magnification at 3000× for each sample are shown in Figure 14. Figure 14a shows that the fresh Fe_2O_3 particles consist of small granulars and grains of about 1−3 μm in size. After reduction, the surface structure and morphology of Fe_2O_3 particles varied. The sizes of the grains increased, and some melted spots were observed when Fe_2O_3 particles were reduced by chars as shown in parts b and c of Figure 14. This was further supported by the Brunauer−Emmett−Teller (BET) areas of the samples. The specific surface areas of the fresh Fe_2O_3 particles and the reduced Fe_2O_3 particles (reduction residue of 3 g of Fe_2O_3 by 0.5 g of K-10-char at the final temperature of 1173 K) are 1.35 and 0.98 m^2/g, respectively. When the final temperature was decreased to 1023 K, as shown in Figure 14d, only slight sintering between the grains was observed and the Fe_2O_3 particles after reduction almost maintained the morphology as that of the fresh Fe_2O_3 particle. It is suggested that the morphology of the Fe_2O_3 particles after reduction is determined by not only the reaction product but also the temperature and the sintering becomes serious when the temperature is increased.

To avoid a high rate of sintering, it may be advantageous to manufacture synthetic iron oxide particles incorporated in a carrier support and binder, which may also improve the reactivity, durability, and longevity of the oxygen carrier particles.[22] Furthermore, iron oxide particles with excellent recyclability are critical to make the process economical.[3]

(43) Hirsch, R. L., Jr.; Lessard, R. R.; Wesselhoft, R. D. Catalytic coal gasification: An emerging technology. *Science* **1982**, *215* (4529), 121–127.
(44) Wang, J.; Sakanishi, K.; Saito, I.; Takarada, T.; Morishita, K. High-yield hydrogen production by steam gasification of hypercoal (ash-free coal extract) with potassium carbonate: Comparison with raw coal. *Energy Fuels* **2005**, *19* (5), 2114–2120.
(45) Ohtsuka, Y.; Asami, K. Steam gasification of coals with calcium hydroxide. *Energy Fuels* **1995**, *9* (6), 1038–1042.
(46) Nahas, N. C. Exxon catalytic coal gasification process—Fundamentals to flowsheets. *Fuel* **1983**, *62* (2), 239–241.
(47) Kühn, L.; Plogmann, H. Reaction of catalysts with mineral matter during coal gasification. *Fuel* **1983**, *62* (2), 205–208.
(48) Bruno, G.; Buroni, M.; Carvani, L.; Del Piero, G.; Passoni, G. Water-insoluble compounds formed by reaction between potassium and mineral matter in catalytic coal gasification. *Fuel* **1988**, *67* (1), 67–72.
(49) Gea, G.; Sanchez, J. L.; Murillo, M. B.; Arauzo, J. Kinetics of CO_2 casification of alkaline black liquor from wheat straw. Influence of CO and CO_2 concentrations on the gasification rate. *Ind. Eng. Chem. Res.* **2004**, *43* (13), 3233–3241.
(50) Hong, S.-J.; Zhang, J.-Y.; Huang, W.-Y.; Lin, J.; Lin, C. Experimental study on catalytic gasification of fujian anthracite with steam using industrial waste liquor alkalis. *J. Fuel Chem. Technol.* **2002**, *30* (6), 481–486.

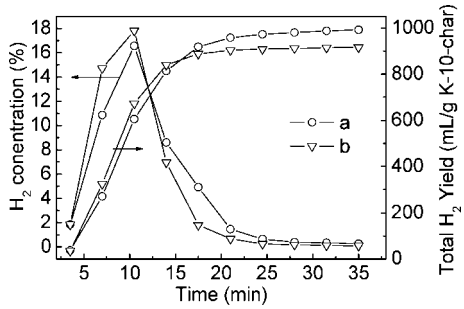

Figure 15. H_2 concentration and cumulative H_2 as a function of time: (a) H_2 production from the residue of 3 g of Fe_2O_3 reduced by 0.5 g of K-10-char with 284 mL/min of Ar and (b) H_2 production from the residue of 3 g of Fe_2O_3 reduced by 0.28 g of K-10-char with 142 mL/min of Ar.

However, the main purpose of this study is to reveal the fundamental possibility of the Fe_2O_3 reduction process. Despite the fact that the present Fe_2O_3 was not optimized, it was able to oxidize all of the carbon in chars adopted in this study.

4.2. H_2 Production through the Steam−Iron Process. The results in section 4.1 indicated that Fe_2O_3 was reduced to FeO and Fe by K-10-char with promising prospect to produce H_2 through the steam−iron process. When the Fe_2O_3 reduction process completed, the fluidizing Ar was adjusted to 284 or 142 mL/min and the reactor temperature was lowered to 1073 K. Once the temperature was stabilized at 1073 K, 0.13 g/min of water was introduced to conduct the steam−iron process to produce H_2.

For both cases as shown in Figure 15, the H_2 concentration reached a peak at 10 min, after that it decreased gradually. For the case that H_2 was produced from the residue of 3 g of Fe_2O_3 reduced by 0.5 g of K-10-char, if it was assumed that Fe_2O_3 was completely reduced to Fe, the total H_2 yield was 1120 mL (normalized to 0.1 MPa and 273.15 K) based on reaction 8 in Table 1, and if it was assumed that Fe_2O_3 was completely reduced to FeO, the total H_2 produced was 280 mL from reaction 9 in Table 1. The total H_2 produced is 1000 mL/g of K-10-char as shown in Figure 15; therefore, the fractions of FeO and Fe in the reduced residue are 43 and 57%, respectively, based on Fe and H_2 conservation. The calorific value of K-10-char is 21.6 MJ/kg, and the low heating value (LHV) of H_2 is 241 kJ/mol.[51] Therefore, the energy efficiency is 50.2% in terms of the energy ratio of H_2/K-10-char. In the case of 3 g of Fe_2O_3 reduced by 0.5 g of K-10-char, the conversion of Fe_2O_3 based on the oxygen in FeO is 71.3%, which agrees well with the value 70.2% obtained using eq 2. For the case that H_2 was produced from the residue of 3 g of Fe_2O_3 reduced by 0.5 g of K-10-char, CO and CO_2 were not observed in the steam−iron process, which indicated that K-10-char was completely converted to CO and CO_2 in the Fe_2O_3 reduction process.

The H_2 yield calculation mentioned above was based on the assumption that FeO and Fe were oxidized to form Fe_3O_4 by steam, which was approved by XRD analysis shown in Figure 16, where the discrete vertical lines were the standard spectra of Fe_3O_4. Figure 16 shows that the XRD spectra of residue of FeO and Fe after the steam−iron process agree with the standard spectra of Fe_3O_4. There are no peaks corresponding to Fe_2O_3 based on the 2θ angles listed in Table 5. The conclusion that FeO and Fe form only Fe_3O_4 rather than Fe_2O_3 can be justified by the thermodynamics analysis of reactions 8 and 9 in Table 1. Oxidation of Fe_3O_4 with steam to Fe_2O_3 is thermodynamically impossible ($\Delta_f G^0$ for the oxidation of Fe_3O_4 to Fe_2O_3 with steam is 103.9 kJ/mol H_2O at $T = 1100$ K); this can only be achieved when oxidation is performed with oxygen.[3,34]

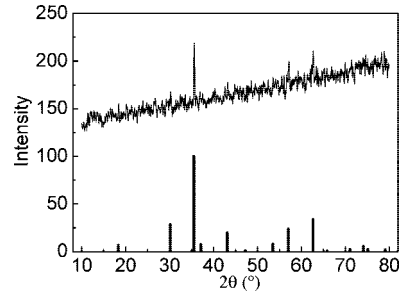

Figure 16. XRD spectra of the residue of FeO and Fe from the steam−iron process.

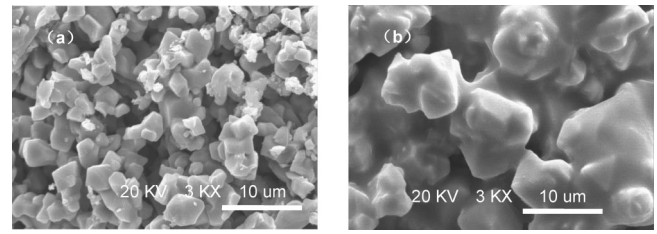

Figure 17. (a) SEM images of FeO and Fe residues after the steam−iron process and (b) residue of Fe_3O_4 oxidized by air at 1073 K.

As shown in Figure 17a, the size of the grains in the residue of FeO and Fe after the steam−iron process is about 5 μm on average, indicating that the grains grow up for the combination with oxygen in steam by comparing the sizes as shown in parts b and c of Figure 14. On the other hand, the BET area of the residue of FeO and Fe after the steam−iron process is 0.0085 m^2/g, which is much smaller than that of the fresh Fe_2O_3 particles. The merge between the grains in the particle was also observed, which may not be caused by a thermal effect because the reaction temperature was 1073 K.

4.3. Fe_3O_4 Oxidation by Air To Produce Fe_2O_3. The oxidation of Fe_3O_4 to Fe_2O_3 may be carried out using air in a conveying system with the removal of heat to generate steam for H_2 production. From stoichiometry consideration, the H_2 production will drop by 11.1% if the transition between Fe and Fe_3O_4 is used instead of Fe to Fe_2O_3.[3] When the steam−iron process completed, the water feed was stopped, the fluidizing Ar was maintained at 142 mL/min, and the reactor temperature was stabilized at 1073 K. Once the reactor was purged clean by Ar, a gas mixture with 8.7 vol % O_2, resulting from 142 mL/min of Ar and 100 mL/min of air with 99.995% purity, was introduced to avoid an excessive temperature increase.

Figure 18 shows the O_2 concentration and temperature profile during the oxidation process of the residue, resulting from the steam−iron process. During the first 5 min, all incoming oxygen reacts with Fe_3O_4. Then, the O_2 concentration increases rapidly during the following 5 min, after which the rise gradually slows down. At last, the O_2 concentration reaches the inlet O_2 concentration at 15 min. The bed temperature increases sharply with time and reaches a peak with 1130 K at about 2.5 min. Then, the temperature decreases gradually and comes back to 1073 K at 6 min. The temperature rise is significantly strong for the exothermic nature of the oxidation reaction 10 as listed in Table 1.

Considerable heat release in a short time will lead to a local deterioration of the iron oxide particles, which is strengthened by the SEM images of the residue of Fe_3O_4 oxidized by air as

(51) Steinfeld, A. Solar hydrogen production via a two-step water-splitting thermochemical cycle based on Zn/ZnO redox reactions. *Int. J. Hydrogen Energy* **2002**, *27* (6), 611–619.

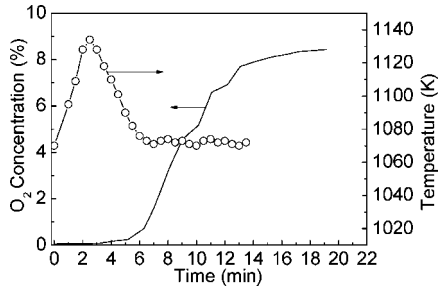

Figure 18. O_2 concentration and temperature profile during the oxidation of Fe_3O_4, resulting from the steam−iron process by air with 8.7 vol % O_2. Fe_3O_4 resulted from 3 g of Fe_2O_3.

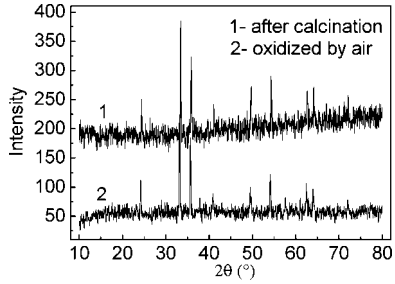

Figure 19. XRD spectra of the Fe_3O_4 residue after oxidation by air.

demonstrated in Figure 17b. The grain size of the residue is about 10 μm on average, indicating subsequent growth of the grains compared to the sizes with 5 μm as shown in Figure 17a. Furthermore, the merge between the grains becomes severe, which is supported by the BET area of the residue of Fe_3O_4 oxidized by air with 0.0013 m^2/g. XRD spectra of the Fe_3O_4 residue after oxidation by air is shown in Figure 19, where the XRD spectra of fresh Fe_2O_3 particles are also given. Figure 19 indicates that Fe_2O_3 was formed when Fe_3O_4 was oxidized by air at 1073 K. Chemical composition comes back to the original Fe_2O_3 after a cycle, but the pore structure and morphology of the Fe_2O_3 particles changed significantly by comparing the image in Figure 17b to that in Figure 14a. The iron oxide particles with good recyclability over multiple redox cycles are required to make the process viable and economical.[3,20] It is worthy of further investigation on the synthesis of Fe_2O_3 particles with excellent recyclability, good mechanical properties, and high reactivity.

The three processes were carried out under atmospheric pressure in this study. However, the processes should be performed at high pressures, aiming at increasing the energy efficiency. Furthermore, in a pressurized system, the recovery of the CO_2 requires only a very small amount of additional power for further compression of the CO_2 to pipeline (3.5 MPa) or sequestration pressure (10 MPa).[52] On the other hand, the effect of pressure on the oxygen carrier and the char reactivity is significantly important.

As the pressure is increased, the reaction rate of the oxygen carrier with gaseous fuel is expected to be increased. However, the experimental results by Garcia-Labiano et al. showed that an increase in total pressure did not lead to an increase in the reaction rate by increasing the partial pressure of the reacting gas; even in some cases, the reaction rate decreased when the total pressure was increased.[52] Therefore, the kinetic parameters necessary to design pressurized CLC systems must be determined at the operating pressure of the industrial system.[52,53]

On the other hand, high pressure is beneficial to the gasification of char by CO_2, but the inhibition of CO becomes significant at higher pressures. Roberts et al. concluded that, at atmospheric pressure, the reaction rate is proportional to the number of surface complexes because the surface of the char is not saturated.[53] As the pressure is increased, more surface complexes are produced, resulting in an increase in the reaction rate. At high enough pressures, the surface will be saturated, such that increases in pressure will not lead to an increase in the reaction rate. When the gasification rate measurements are investigated under process conditions, where significant product gas inhibitions or pore diffusion are important, more attentions should be pay to the effects of total and partial pressure of the reactant pressure on the reaction kinetic parameters especially for the direct reduction of Fe_2O_3 by char, where CO and CO_2 are formed.

5. Conclusions

The following conclusions were made from the above study:

The feasibility of the three processes including direct reduction of iron oxide by char (without a gasifying agent) based on CLC, H_2 production by the steam−iron process, and the oxidation of Fe_3O_4 resulting from the steam−iron process to the original Fe_2O_3 by air was supported by the experimental results carried out using a fluidized-bed reactor.

Char resulting from the lignite loaded with K_2CO_3 was used successfully as a reducing material, leading to the reduction of Fe_2O_3 to FeO and Fe with fractions of 43 and 57%, respectively, in the case of 3 g of Fe_2O_3 and 0.5 g of K-10-char, where the conversion of Fe_2O_3 was 70.2%. The reduction of Fe_2O_3 by K-10-char at 1073 K is desirable from the perspective of the carbon conversion rate and high concentration of CO_2. The oxidation rate of K-10-char by Fe_2O_3 without a gasifying agent was comparable to the steam gasification rate of K-10-char.

FeO and Fe produced from the Fe_2O_3 reduction of char were feasible for H_2 production through the steam−iron process. The total H_2 produced was 1000 mL of H_2/g of K-10-char, where the energy efficiency was 50.2% in terms of the energy ratio of H_2/K-10-char.

Fe_3O_4 resulting from the steam−iron process was successfully oxidized by air to the original Fe_2O_3, and it took about 15 min because Fe_3O_4 resulting from 3 g of Fe_2O_3 was oxidized to Fe_2O_3 by air with an 8.7 vol % O_2 concentration at 1073 K.

Acknowledgment. This study was supported by The National Basic Research Program of China (2006CB705807) and the National High Technology Research and Development Program of China (2003AA501330).

EF800014R

(52) Garcia-Labiano, F.; Adanez, J.; de Diego, L. F.; Gayan, P.; Abad, A. Effect of pressure on the behavior of copper-, iron-, and nickel-based oxygen carriers for chemical-looping combustion. *Energy Fuels* **2006**, *20* (1), 26–33.

(53) Roberts, D. G.; Harris, D. J. Char gasification with O_2, CO_2, and H_2O: Effects of pressure on intrinsic reaction kinetics. *Energy Fuels* **2000**, *14* (2), 483–489.